
Article:
Lawal, J., Kiryukhantsev-Korneev, P., Matthews, A. et al. (1 more author) (2017) Mechanical properties and abrasive wear behaviour of Al-based PVD amorphous/nanostructured coatings. Surface and Coatings Technology, 310. pp. 59-69. ISSN 0257-8972

https://doi.org/10.1016/j.surfcoat.2016.12.031

Mechanical Properties and Abrasive Wear Behaviour of Al-based PVD Amorphous/Nanostructured Coatings

J. Lawal[1], P. Kiryukhantsev-Korneev[2], A. Matthews[3] and A. Leyland[1]

[1] Department of Materials Science and Engineering, University of Sheffield, Sheffield S1 3JD, UK.

[2] National University of Science and Technology "MISIS" Scientific-educational Center of SHS, Leninsky Prospect 4, Moscow 119049, Russia.

[3] Pariser Building - B24 ICAM, School of Materials, The University of Manchester, Manchester, M13 9PL, UK

Corresponding author: a.leyland@sheffield.ac.uk

Abstract

This study examines the mechanical properties and wear characteristics of aluminium-based nanostructured coatings produced by magnetron sputtering in an argon/nitrogen plasma. Compositional analysis of AlNiTiSiB(N) coatings was carried out by glow discharge optical emission spectroscopy (GDOES). Scanning electron microscopy (SEM), transmission electron microscopy (TEM) and X-ray diffraction (XRD) were used to study the structure of the coatings; hardnesses and elastic moduli were also determined. The abrasive wear behaviour of the coating-substrate system was studied using a slurry micro-abrasion wear test. Nitrogen-free (AlNiTiSiB) coatings were found to be surprisingly hard and wear resistant; however, nitrogen incorporation had a significant influence on mechanical properties and abrasion resistance, with increased hardness (from 8 to 15 GPa) and a significant reduction in wear coefficient – from 6 x 10^{-3} mm^3/Nm for a nitrogen-free coating (0B), to approximately 1.5 x 10^{-3} mm^3/Nm, for a coating deposited at 15 sccm nitrogen gas flow rate (15T) – being observed in

the various AlNiTiSiB(N) coatings investigated. Several of the coatings were found to be comparable to convention ceramic PVD hard coatings (e.g. CrN) in terms of resistance to abrasion.

Keywords: PVD nanostructured coatings; Al-based coatings; abrasive wear; mechanical properties

1. Introduction

Aluminium-based films deposited by physical vapour deposition (PVD) have excellent potential to act as replacements for toxic electroplated coatings such as cadmium and hard-chromium; also for electroless nickel and for hard-anodizing of aluminium alloys. However, it is well known that pure aluminium alone is too chemically electronegative to provide reliable and uniform sacrificial protection to steel; it tends also to exhibit poor mechanical/tribological properties. In addition, there are technical challenges in depositing high-integrity alloyed coatings (with improved mechanical/electrochemical behaviour) by conventional techniques such as thermal spraying and Ion Vapour Deposition (IVD [1]), the latter also known as 'Ivadizing'.

Although aluminium-based coatings have the potential to replace traditional electroplated metallic layers (e.g. for sacrificial corrosion protection of steels & other alloy substrates) [2], the mechanical/tribological properties of pure Al are poor and there are challenges in depositing alloyed coatings [3]. For example, IVD-Al (resistive wire evaporation in diode argon plasma) has been used for many years as a cadmium-replacement coating on aircraft components; however, the technical scope of the process is somewhat limited. Harder Al-

alloy films (such as Al-5Mg) deposited by IVD are difficult to post-coat shot peen (needed for coating densification & sizing) [4]; also, IVD-Al generally requires (as does cadmium) chemical post-treatments – such as chromating (which is also highly toxic) – to perform effectively in corrosion applications. Nanostructured metallic aluminium-alloy coatings (deposited by enhanced-plasma PVD methods) have the potential to partially replace cadmium, remove the need for chromating and (if sufficiently hard & wear-resistant) may also be candidates to replace other potentially hazardous coatings/treatments used for tribological applications where corrosion is also an issue.

It has previously been demonstrated by Matthews, Leyland and co-workers [5-7] that PVD metallic coatings based on (for example) Cr or Ti can, with suitable alloying additions, yield surprisingly high values of hardness (≥ 12-15 GPa) whilst retaining low Young's modulus – making such coatings tough and compliant. The useful mechanical and tribological properties of these types of PVD film have been clearly demonstrated [5, 8, 9] and often relate to the generation of nanocrystalline – or mixed crystalline/amorphous – phases in the deposited coating (either during or after deposition). Veprek [10] established a concept of superhard nanocomposite coatings (composed of a hard nanocrystalline phase embedded in a compliant amorphous intergranular phase), in which one of the main principles was to postpone (or avoid) the known fracture mechanisms of crystalline and amorphous materials. However, PVD nanostructured coatings based on the (largely ceramic) phase constituents commonly investigated so far are unlikely to be useful where combined wear and corrosion protection (particularly for the galvanic/sacrificial corrosion protection often required by industry) are important considerations. Nonetheless, a major challenge in developing 'adaptive' coatings (which provide excellent functionality in diverse environments) is to be able to manipulate satisfactorily their nanostructure [11].

This work is focused on the development of aluminium-based metallic PVD nanostructured/amorphous coatings with multifunctional and adaptive properties. These coatings are intended to suit a variety of technically challenging environments – and impart a range of beneficial features which (for example) IVD-aluminium, although arguably more environmentally friendly than aqueous bath plated alternatives, is still unable to provide. Here we present the mechanical and abrasive wear properties of a range of sputtered-AlNiTiSiB PVD coatings with chemical compositions determined both by position in front of a composite $Al_{75}Ni_{25}/Ti_{28}Si_{17}B_{55}$ segmented target and by different nitrogen reactive gas flow rates during coating deposition.

These coatings have the potential to replace electroplated cadmium and hard chromium, electroless nickel, hard anodising (for aluminium) and other 'traditional' coatings used in corrosion and/or wear protection for aerospace, automotive and other engineering applications – where environmental legislation is restricting the use of many of the toxic materials and processes typically required to deposit (and/or to functionalise) such coatings.

2. Experimental Procedure

Nitrogen-free – or nitrogen-containing – AlNiTiSiB coatings were deposited by direct – or reactive – magnetron sputter deposition on polished rectangular (50 x 25 x 2 mm) AISI 304 austenitic stainless steel test coupons, in an argon – or argon/nitrogen – low-pressure glow discharge. Fig. 1 shows a schematic plan view of the deposition chamber with the magnetron holding four sputter target segments; the uppermost two (each being 75 x 100 x 6 mm) were of a Ti-Si-B ceramic compound and the other two (being 80 x 100 x 6 mm and 150 x 100 x 6 mm, respectively) were of an Al_3Ni intermetallic compound. Overall sputter target dimensions of 380 x 100 x 6 mm were

achieved with this design. Table 1 provides a summary of the individual and overall compositions of the sputter target materials. The stainless steel substrate holder was mounted at a distance of approximately 100 mm from the sputter target. The rectangular substrate coupons were first washed in acetone, then cleaned ultrasonically in isopropanol for 15 min. Sputter cleaning of the substrates was carried out for 20 min in an argon plasma at approximately 3.0 Pa gas pressure, with a negative bias of –600 V applied to the substrate holder. The segmented target was then pre-conditioned for 40 min at approximately 0.3 Pa argon gas pressure and 1500 W power, to arrive at a target voltage of –430 V (while shielding the substrates with a shutter). Coatings were deposited at around 0.3 Pa total gas pressure and at 1500 W target power, with the target voltage pulsed at a frequency of 150 kHz. Although it was difficult to record directly the substrate temperature during the coating runs (because of the target/substrate/shutter configuration used), the substrate temperature is unlikely to be (in any stage of the process) less than 150^{o}C, or more than 250^{o}C; most probably it would be in the range of 200 ± 20^{o}C during coating deposition, based on the specific parameters selected. This is based on the previous work done on the same equipment using similar deposition parameters [12-14]. In order to increase ion bombardment at the substrate, thereby improving coating adhesion, the substrate holder was biased negatively at –50 V DC and deposition was carried out for 120 min to obtain coating thicknesses in the range of 7 – 14 μm. Coatings of a wide range of chemical compositions were produced by placing the abovementioned stainless steel coupons at three different positions in front of the segmented target (see Fig. 1) and, in each deposition cycle, choosing different nitrogen flow rates between 0 and 20 sccm. Coated sample designations are presented in Table 2.

GDOES coating composition depth profiling was carried out using a Profiler 2 device (Horiba Jobin Yvon, France) operating at frequency of 13.56 MHz. GDOES machines can work in three regimes: DC, RF and Pulsed-RF (to minimize the thermal gradient during etching); RF

mode was used for this work. This was used for elemental compositional analysis and also to confirm coating thicknesses. Table 3 presents the chemical compositions of the coatings produced.

A Siemens D5000 X-ray diffractometer (Cu Kα radiation at 40 kV and 40 mA) was used to collect X-ray diffraction (XRD) coating phase constitution data (using both θ/2θ and glancing-angle modes; with incident angle of 2^{o} for the latter). A Bruker D2 Phaser X-ray diffractometer (Cu Kα radiation at 30 kV and 10 mA) was used to collect θ/2θ XRD data of the annealed samples. XRD profile simulation was carried out using the International Centre for Diffraction Data (ICDD) 'PDF-4+' database (version 4.15.0.5) and 'SIeve+' fitting software.

An FEI Inspect-F scanning electron microscope (SEM) was used to obtain secondary electron images of focussed ion beam (FIB) machined and fracture cross-sections of each coating. Samples for transmission electron microscopy (TEM) were also prepared by in-situ ion milling of FIB sections using a Quanta 200 3D dual-beam FIB-SEM microscope running at 20 kV electron acceleration voltage and 30 kV gallium ion beam voltage. To minimise structural damage by the gallium ions, a gold layer (~ 35 nm thick) was deposited on the surface of all samples. This was carried out prior to the in-situ deposition of a carbon coating (2 μm thick) in the Quanta 200 3D dual-beam FIB-SEM instrument. Electron diffraction patterns were obtained from milled FIB sections using a Philips EM420 instrument (120 kV acceleration voltage).

A Hysitron Inc. Triboscope™ was used to evaluate coating hardness and elastic modulus. Multiple indentations were made on each sample using a Berkovitch triangular pyramidal

diamond indenter at a maximum penetration depth of < 10% of the coating thickness. The results presented in section 3 represent average values obtained from nine measurements made on each coating sample.

A Plint TE-66 micro-scale abrasion tester was used to evaluate the resistance of the coatings to slurry abrasion in a rotating-sliding ball-on-plate contact. This test was carried out using a silicon carbide aqueous slurry (F1200, ~3-4 μm particle size), with SiC concentration of ~80g/100ml of distilled water. A 25 mm diameter SAE 52100 steel ball was used to transport the slurry, creating a crater of approximately hemispherical geometry in the coating. The ball was rotated at a tangential velocity of 0.1 ms^{-1} for 100 revolutions while applying a 0.2 N load. This test was used to evaluate wear coefficients of six AlNiTiSiB(N) coatings selected for study; a CrN ceramic coating and an uncoated AA6082 aluminium alloy were also evaluated (for comparison purposes). Slurry concentration and normal load parameters were chosen to ensure a three-body rolling wear regime (rather than two-body grooving or mixed two-body/three-body) – primarily for ease of crater volume measurement [15-21]. A Veeco Dektak 150 surface profiler was used to obtain depth profiles of each wear crater; crater diameter was estimated using optical microscope and wear coefficient (k) was evaluated using the formula for estimating k as described in equation 6 in [15]. Annealing experiments were carried out at $600^{o}C$ using radiant heating under high vacuum in an electron-beam PVD chamber, pumped down to 10^{-5} mbar. The holding time was 2hrs; samples were then vacuum-cooled to room temperature. Open Circuit Potential (OCP) measurements on selected coatings were carried out for 120 min using a Solartron 1286 potentiostat in 3.5 wt. % NaCl aqueous solution at ambient temperature.

3. Results and Discussion

3.1 Coating composition, structure and morphology

Amorphous and (in some cases) partially nanocrystalline AlNiTiSiB(N) coatings were produced – as confirmed by XRD data and TEM electron diffraction patterns (Fig. 2), with composition variations depending on two key factors: first, the chosen nitrogen flow rate (0 – 20 sccm) and second, the position of the substrate on the sample holder (top, middle or bottom). As seen in Fig. 1, the top (T) samples were directly facing only the TiSiB segment of the target. The middle (M) samples were overlapping the two target materials (i.e. partially TiSiB and, mainly, Al_3Ni), while the bottom (B) samples were facing only the Al_3Ni segment. However, gas scattering over the 100 mm source-to-substrate distance ensured that most (if not all) coatings produced contained all elements present in the target segments (except for a few of the bottom samples, where the Si content was unmeasurably low).

As expected (see Table 3 below), the nitrogen content in the coatings increased systematically with increasing nitrogen reactive gas flow rate. The atomic percentage of Al and Ni also increased systematically from the top coating to the bottom coating in each coating run. However, the higher the nitrogen content in the coatings, the lower the amount of incorporated Al and Ni. Although the amount of Ti present in the coatings was also affected by sample position (as well as the nitrogen flow rate), it exhibited an opposite trend compared to Al and Ni; with the highest levels seen in the top samples. Silicon behaved similarly to boron in this set of coatings. The atomic percentages of Si and B exhibited a continuous decrease from top to bottom coating – and with increasing nitrogen flow rate; it was also observed that all bottom samples contained insignificant amounts of Si, with 10B, 15B and 20B samples showing ‘zero’ Si content under GDOES measurement.

As mentioned previously, the coatings deposited were either fully amorphous or partially nanocrystalline. Although (as might be expected from the above) it is difficult to index the broad XRD 'peak' typically seen at $35^{o} < 2\theta < 55^{o}$, this range of 2θ is populated by many of the reflections attributable to metallic Al, Ni and intermetallic Al-Ni phases. Fig. 3a reveals that 13 reflections in the 2θ range where the 'peak' is located belong to Al_3Ni; the crest of the peak (at $2\theta \sim 44^{o}$) also coincides with one of the main Al_3Ni peaks. In addition, the combined atomic percentage of Al and Ni in (for example) 0B coating (where TEM analysis reveals a significant level of nanocrystallinity) is ~88% and in an approximate 3:1 Al:Ni ratio, making the formation of significant quantities of Al_3Ni in the coating a likely outcome. One of the XRD profiles (1 nm crystallite size simulation) of Al_3Ni intermetallic phase (Fig. 3b) shows a similar XRD profile to that of the 0B coating shown in Fig. 3a. Therefore, we can cautiously assign the broad peak in the XRD profile of 0B to an ultrafine nanocrystalline Al_3Ni intermetallic phase, with crystallite sizes in the range of only a few nanometres (i.e < 2 nm, comparing the shape of the XRD profile of 0B to the simulated XRD profiles of Al_3Ni shown in Fig. 3b. In addition, the amorphous 'bump' at $2\theta = 20^{o} - 30^{o}$ also coincides with strong Al_3Ni reflections (see XRD profile simulated for 50 nm crystallite size shown in Fig. 3b).

Although a detailed study of the thermal stability of the AlNiTiSiB(N) coatings produced is beyond the scope of this paper, it is worth including the XRD (θ/2θ) scans – for 2θ ranging from 0^{o} to 60^{o} – for coatings 0B and 15T, annealed to 600^{o}C (Figs. 4a and 4b), in order to further confirm the likely structure and phase composition of the AlNiTiSiB(N) coatings presented in this paper. Note firstly, the close similarity between the XRD profile of Al_3Ni (simulated for 50 nm crystallite size) shown in Fig. 3b and that of annealed 0B coating shown

in Fig. 4a. However, the peaks shown in Fig. 4a are broader than those in the 50 nm crystallite size simulated profile (and somewhat narrower than those simulated at 10 nm); this suggests that the average crystallite size for the annealed 0B coating is < 50 nm (and most probably in the 20 – 30 nm range).

Note secondly, that the 15T coating, annealed at 600^{o}C, (Fig. 4b) remains amorphous – and remarkably stable at high temperature – with just slight retexturing of the underlying AISI 304 substrate (and no obvious coating devitrification).

The coatings generally show a dense and featureless morphology (as seen in Figs. 5 and 6 below) with thicknesses ranging from 7 – 14 μm (from top to bottom) in each coating run. The observed coating thickness range occurs as a result of differences in sputter yield of the target elements due to physical and electrical properties of the sputter target materials used – the Al-Ni target segment is intermetallic, while the Ti-Si-B segment (although electrically conductive) is predominantly ceramic. The sputter target layout adopted for coating deposition was deliberately configured to produce as wide a range of coating compositions as possible (over which the wear and corrosion properties could be examined and 'tuned'), rather than to obtain uniformly constant deposition rates.

3.2 Mechanical Properties

Fig. 7 shows the variations in coating hardness (H) and elastic modulus (E) as the nitrogen content is increased. Fig. 7a shows an appreciable decrease in both hardness (H) and elastic modulus (E) of the coatings from position T (samples close to the TiSiB target segment) to position B (samples close to Al_3Ni target segment). The coatings with no added nitrogen had

hardnesses ranging from 13 GPa (0T) to 8 GPa (0B); elastic modulus also decreased significantly from 172 GPa (0T) to 135 GPa (0B). At 10 sccm N_2 flow, hardness decreased moderately from 15 GPa (position T coating) to 13 GPa (position B coating); however, coatings at positions T and M had similar hardness values – as well as showing similar elastic moduli (Fig. 7b). The elastic moduli for the 15 sccm N_2 flow coatings show a similar trend to those observed in the 10 sccm N_2 flow coatings, with values varying from approximately 150 to 180 GPa. However, there was no change in H from position T to B at 15 sccm N_2 flow – although E decreased significantly from 177 to 151 GPa from position M to B (Fig. 7c).

A combination of factors is responsible for the relatively high hardnesses observed in general for the AlNiTiSiB coatings, as-deposited. The diverse physical properties of the individual elements incorporated in the coatings had a significant influence in promoting amorphisation and – as a consequence – on the measured mechanical properties. The relatively high hardness and high modulus of compounds formed by the elements in the TiSiB sputter target were responsible for the H and E values observed in the top (T) coatings and this group of coatings are collectively somewhat harder than their middle (M) and bottom (B) counterparts. The presence of boron in all the coatings undoubtedly has a positive impact on achieving high coating hardness. However, the effect of boron is most pronounced in coating 0T, where it is the second most abundant element (after aluminium); with a measured boron atomic concentration of ~26%, a coating hardness value of 13 GPa is perhaps not a surprising outcome. The calculated hardness and elastic modulus of coating 0B are in accordance with literature data for Al_3Ni (being ~8 GPa and between 116 and 152 GPa, respectively) [22-24] which, as the coating chemical composition shown in Table 3 would suggest (and as Figure 2 and 3 confirm) is the main (ultra-fine) nanocrystalline constituent phase of the 0B coating. In addition to the foregoing, the ultra-fine nanostructure of the nitrogen-free coatings was also

partially responsible for their relatively high hardness (XRD shows evidence of grain sizes in the lower nanometer range, Figs. 2 and 3), due to a combination of Hall-Petch effects (i.e. hardening at grain sizes above 20 – 30 nm and possibly 'inverse' softening at ultra-fine grain sizes [25]) and probable delocalisation of shear-band activity (in the amorphous component of the coating) due to the presence of local short-range nanocrystallinity.

For the nitrogen-containing coatings, the combined effect of boron and nitrogen resulted in ultra-fine grain size for some of these coatings – as well as the completely amorphous structure observed in others (as evidenced by the broad, shallow peak seen in the XRD patterns of Fig.2). Coating 15T, although showing similar hardness as 15M and 15B, exhibits wear behaviour which differs significantly to that of 15M or 15B. Although it might be expected that 15T would show hardness higher than 15 GPa, the completely amorphous structure of this coating most probably resulted in a (relative) loss of hardness due to the effects of shear-band localisation which are often reported for fully amorphous materials during deformation [11, 26-28]. However, 15T still showed the best resistance to abrasion (see discussion in section 3.3), with respect to all other coatings in this study, due in part to its higher modulus (E_{15T} of 180 GPa, compared to 177 GPa and 151 GPa for E_{15M} and E_{15B} respectively), which is closely matched (rather than lower) to that of the stainless steel substrate. For ceramic hard coatings, E is often much higher that of the substrate (i.e. the opposite to typical values expected for Al-based metallic thin film [11, 26, 29]

The surprising mechanical properties of these Al-based coatings (that is, their relatively high hardness, approaching almost ceramic hardness levels, yet with elastic moduli lower than that of a typical steel substrate material) translates into the excellent wear behaviour seen in (most of) these coatings.

3.3 Abrasive Wear Behaviour

In this study, six of the fifteen coating samples were chosen for abrasive wear evaluation, selected primarily on the basis of promising electrochemical behaviour (range of suitable open circuit potential values) and sliding wear data (not reported in this work).

Fig. 8 shows a comparison of the abrasive wear behaviour of selected AlNiTiSiB(N) metallic coatings in comparison with an (uncoated) aluminium alloy 6082 substrate and a CrN PVD ceramic coating. Even the nitrogen-free coating (0B) shows abrasion resistance noticeably superior to that of the AA6082 substrate; however, all selected nitrogen-containing coatings exhibit excellent wear resistance, with values being comparable to that of a conventional ceramic hard coating (i.e. PVD CrN – 1.4 X 10^{-3} mm^3/Nm under identical test conditions).

The SEM images (of 3 selected, representative coatings) in Fig. 9 clearly show a three-body 'rolling' abrasive wear regime in each case. These images show that the wear behaviour was essentially identical for 'high', 'medium', and 'low' wear rate coatings, with the mechanism being predominantly one of mild indentation/plastic tearing, with small numbers of short micro cracks also being formed. The dimensions of the indentation features observed are comparable to the size of the SiC particles used to perform the test. However, in comparison with the other Al-based coatings in this study, 0B in particular showed somewhat more severe wear, with a wear coefficient over twice that of coating 10B and almost four times that of coating 15T. Fig. 9 also includes images of the worn surface of uncoated aluminium alloy (AA6082) and PVD CrN coating (both shown for comparison). There is clearly a gradual

trend from more ductile (micro-tearing) to more brittle (micro-fracture) wear behaviour from top to bottom; however, no obvious change in the underlying wear regime can be identified.

Fig. 10 illustrates the (approximately) hemispherical geometry of the abrasion wear craters produced. Judging from the thicknesses of the coatings selected for this study (7 to 14 μm), Fig. 10 also reveals that all micro-abrasion tests were non-perforating, making it possible to evaluate reliably the wear resistance of the coatings without the influence of the stainless steel substrate. However, it should also be noted that (according to the individual crater dimensions) coatings 15M and 15T appear respectively to exhibit wear volumes comparable to, or somewhat lower than, that of CrN – which does not correlate with the calculated wear coefficients in Fig. 8. The reason for this discrepancy (albeit small) is not clear – despite detailed cross-checking of the data.

It should also be mentioned that, in addition to surprisingly good abrasive wear resistance, the AlNiTiSiB(N) coatings reported here yield (depending on the chemical composition) open circuit potentials ranging from −0.30 to −0.65 V (selected examples shown in Table 4 [29]), making them excellent candidates for sacrificial corrosion protection of many steels.

An overall summary of the main relevant properties of the six coatings chosen for this study is shown in Table 4 [29], demonstrating the potential to adjust the properties of AlNiTiSiB(N) coatings to suit different engineering applications and environments.

Conclusions

Partially nanostructured and fully amorphous Al-based PVD metallic coatings have been deposited with high hardness (previously unattained for such Al-rich metallic thin films), ranging from 8 – 15 GPa and low elastic modulus, ranging from 135 – 180 GPa; i.e. similar to (or somewhat lower than) that of the chosen steel substrate material.

As well as imparting excellent tribological behaviour in their own right, the combined mechanical and tribological properties of the AlNiTiSiB(N) coatings also offer the opportunity to use such thin film materials as compliant, but durable, interlayers (with adjustable electrochemical behaviour) for a wide range of PVD graded/multilayered coating systems.

The coatings reported here in general show surprisingly good abrasion resistance (comparable in most cases to that of a typical PVD ceramic coating such as CrN) across a wide range of chemical compositions – with the latter consideration providing considerable scope to tune (and match) coating/substrate electrochemical behaviour, to provide good long-term galvanic (sacrificial) corrosion protection to a range of engineering alloy substrate materials – in addition to the required mechanical/tribological properties.

The combination of good mechanical, tribological and galvanic corrosion properties exhibited by PVD AlNiTiSiB(N) metallic coatings opens up the potential to select more cost-effective substrates for engineering applications. This is achievable, since such metallic PVD coatings can be deposited with good integrity at relatively high rates to a thicknesses in excess of 10μm, whilst also providing improved load-bearing capacity to low-alloy and non-ferrous substrate materials, as well as to the stainless steel substrate material towards which this initial study was directed.

Acknowledgements

The authors are grateful for financial support from the following institutions: Tertiary Education Trust Fund (TETFUND) Nigeria, University of Lagos, Nigeria, Schlumberger Faculty for the Future, Engineering and Physical Sciences Research Council (EPSRC), UK, TS/H000658/1 and Russian Scientific Foundation (Project No. 15-19-00203), Russia.

References

1. Holmes V., Muehlberger D., and Reilly J., The Substitution of IVD (ion vapor deposition) aluminum for cadmium, 1989, DTIC Document.

2. Kautek W., The galvanic corrosion of steel coatings: aluminum in comparison to cadmium and zinc. Corrosion Science, 1988. **28**(2): p. 173-199.

3. Monaghan D. P., Teer D. G., Logan P. A., Laing K. C., Bates R. I., and Arnell R. D., An improved method for the deposition of corrosion-resistant aluminium coatings for aerospace applications. Surface and Coatings Technology, 1993. **60**: p. 592-596.

4. Alanazi N. M., Leyland A., Yerokhin A. L., and Matthews A., Influence of Mg addition on corrosion behavior of ion vapor deposited al coatings. Materials Performance, 2014. **53**(12): p. 40-45.

5. Baker M. A., Kench P. J., Joseph M. C., Tsotsos C., Leyland A., and Matthews A., The nanostructure and mechanical properties of PVD CrCu(N) coatings. Surface and Coatings Technology, 2003. **162**: p. 222-227.

6. Rebholz C., Schneider J. M., Leyland A., and Matthews A., Wear behaviour of carbon-containing tungsten coatings prepared by reactive magnetron sputtering. Surface and Coatings Technology, 1999. **112**(1-3): p. 85-90.

7. Rebholz C., Ziegele H., Leyland A., and Matthews A., Structure, mechanical and tribological properties of nitrogen-containing chromium coatings prepared by reactive magmetron sputtering. Surface and Coatings Technology, 1999. **115**: p. 222-229.

8. Rebholz C., Schneider J. M., Voevodin A. A., Steinebrunner J., Charitidis C., Logothetidis S., Leyland A., and Matthews A., Structure, mechanical and tribological properties of sputtered TiAlBN thin films. Surface and Coatings Technology, 1999. **113**(1-2): p. 126-133.

9. Tsotsos C., Kanakis K., Davison A., Baker M. A., Matthews A., and Leyland A., Mechanical and tribological properties of CrTiCu(B,N) glassy-metal coatings deposited by reactive magnetron sputtering. Surface and Coatings Technology, 2006. **200**: p. 4601-4611.

10. Veprek S., Conventional and new approaches towards the design of novel superhard materials. Surface and Coatings Technology, 1997. **97**(1-3): p. 15-22.

11. Leyland A. and Matthews A., Design criteria for wear-resistant nanostructured and glassy-metal coatings. Surface and Coatings Technology, 2004. **177-178**: p. 317-324.

12. Audronis M., Jimenez O., Leyland A., and Matthews A., The morphology and structure of PVD ZrN–Cu thin films. Journal of Physics D: Applied Physics, 2009. **42**(8): p. 085308.

13. Audronis M., Leyland A., Matthews A., Kiryukhantsev-Korneev F. V., Shtansky D. V., and Levashov E. A., The Structure and Mechanical Properties of Ti-Si-B Coatings Deposited by DC and Pulsed-DC Unbalanced Magnetron Sputtering. Plasma Processes and Polymers, 2007. **4**(S1): p. S687-S692.

14. Audronis M., Leyland A., Matthews A., Wen J. G., and Petrov I., Characterization studies of pulse magnetron sputtered hard ceramic titanium diboride coatings alloyed with silicon. Acta Materialia, 2008. **56**(16): p. 4172-4182.

15. Rutherford K. L. and Hutchings I. M., A micro-abrasive wear test, with particular application to coated systems. Surface and Coatings Technology, 1996. **79**(1–3): p. 231-239.

16. Rutherford K. and Hutchings I., Theory and application of a micro-scale abrasive wear test. Journal of Testing and Evaluation, 1997. **25**(2): p. 250-260.

17. Trezona R. I., Allsopp D. N., and Hutchings I. M., Transitions between two-body and three-body abrasive wear: Influence of test conditions in the microscale abrasive wear test. Wear, 1999. **225-229**(I): p. 205-214.

18. Adachi K. and Hutchings I. M., Wear-mode mapping for th micro-scale abrasion test. Wear, 2003. **255**(1-6): p. 23-29.

19. Gee M. G., Gant A., Hutchings I., Bethke R., Schiffman K., Van Acker K., Poulat S., Gachon Y., and von Stebut J., Progress towards standardisation of ball cratering. Wear, 2003. **255**(1-6): p. 1-13.

20. Gee M. G., Gant A. J., Hutchings I. M., Kusano Y., Schiffman K., Van Acker K., Poulat S., Gachon Y., Von Stebut J., Hatto P., and Plint G., Results from an interlaboratory exercise to validate the micro-scale abrasion test. Wear, 2005. **259**(1-6): p. 27-35.

21. Cassar G., Banfield S., Avelar-Batista Wilson J. C., Housden J., Matthews A., and Leyland A., Micro-abrasion wear testing of triode plasma diffusion and duplex treated Ti-6Al-4V alloy. Wear, 2012. **274-275**: p. 377-387.

22. Ke L., Huang C., Xing L., and Huang K., Al–Ni intermetallic composites produced in situ by friction stir processing. Journal of Alloys and Compounds, 2010. **503**(2): p. 494-499.

23. Miranda G., Madeira S., Silva F. S., and Carvalho O., A nanoindentation study on Al3Ni interface of Ni reinforced Aluminum-Silicon composite, in Mechanics of Advanced Materials and Structures2016, Taylor & Francis. p. 00-00.

24. Wang S. H., Uan J. Y., Lui T. S., and Chen L. H., Examination on the aging and tensile properties of Al-Zn-Mg/Al3Ni eutectic composite. Metallurgical and Materials Transactions A, 2002. **33**(3): p. 707-711.

25. Konstantinidis D. A. and Aifantis E. C., *On the "Anomalous" hardness of* nanocrystalline materials. Nanostructured Materials, 1998. **10**(7): p. 1111-1118.

26. Leyland A. and Matthews A., On the significance of the H/E ratio in the wear control: a nanocomposite coating approach to optimised tribological behaviour. Wear, 2000. **246**: p. 1-11.

27. Greer A. L., Rutherford K. L., and Hutchings I. M., Wear resistance of amorphous alloys and related materials. International Materials Reviews, 2002. **47**(2): p. 87-112.

28. Greer A. L., Cheng Y. Q., and Ma E., Shear bands in metallic glasses. Materials Science and Engineering: R: Reports, 2013. **74**(4): p. 71-132.

29. Lawal J. T., Physical Vapour Deposition of Aluminium-Rich Metallic Nanostructured/Amorphous Coatings for Wear and Corrosion Protection: PhD Thesis, Department of Materials Science and Engineering, University of Sheffield, Submitted 2016.

List of figures

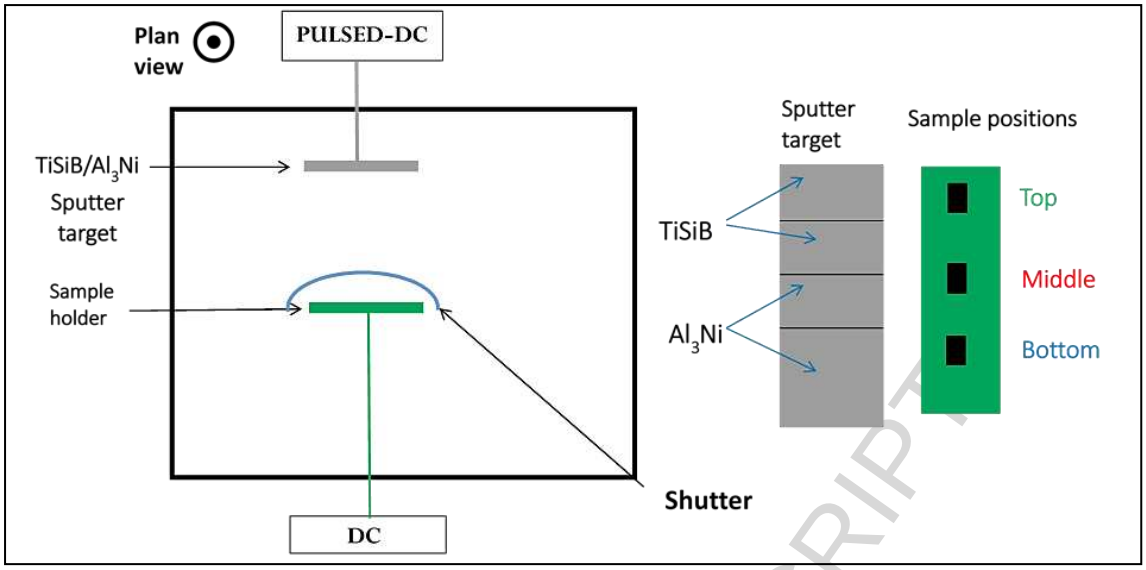

Fig. 1

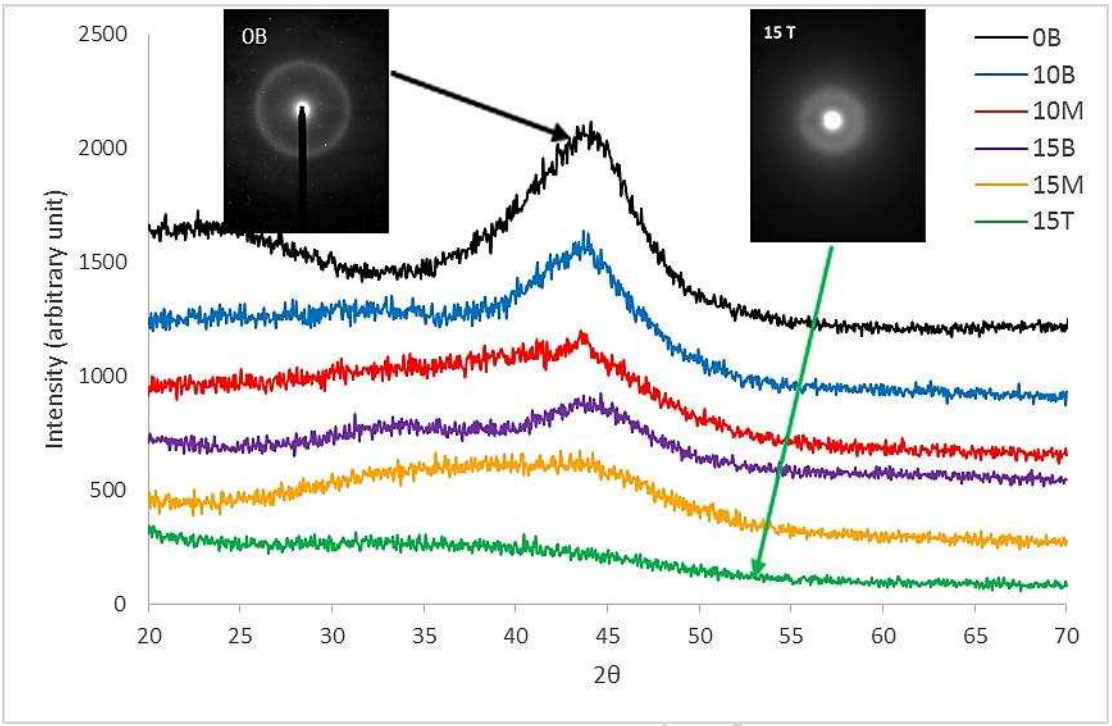

Fig. 2

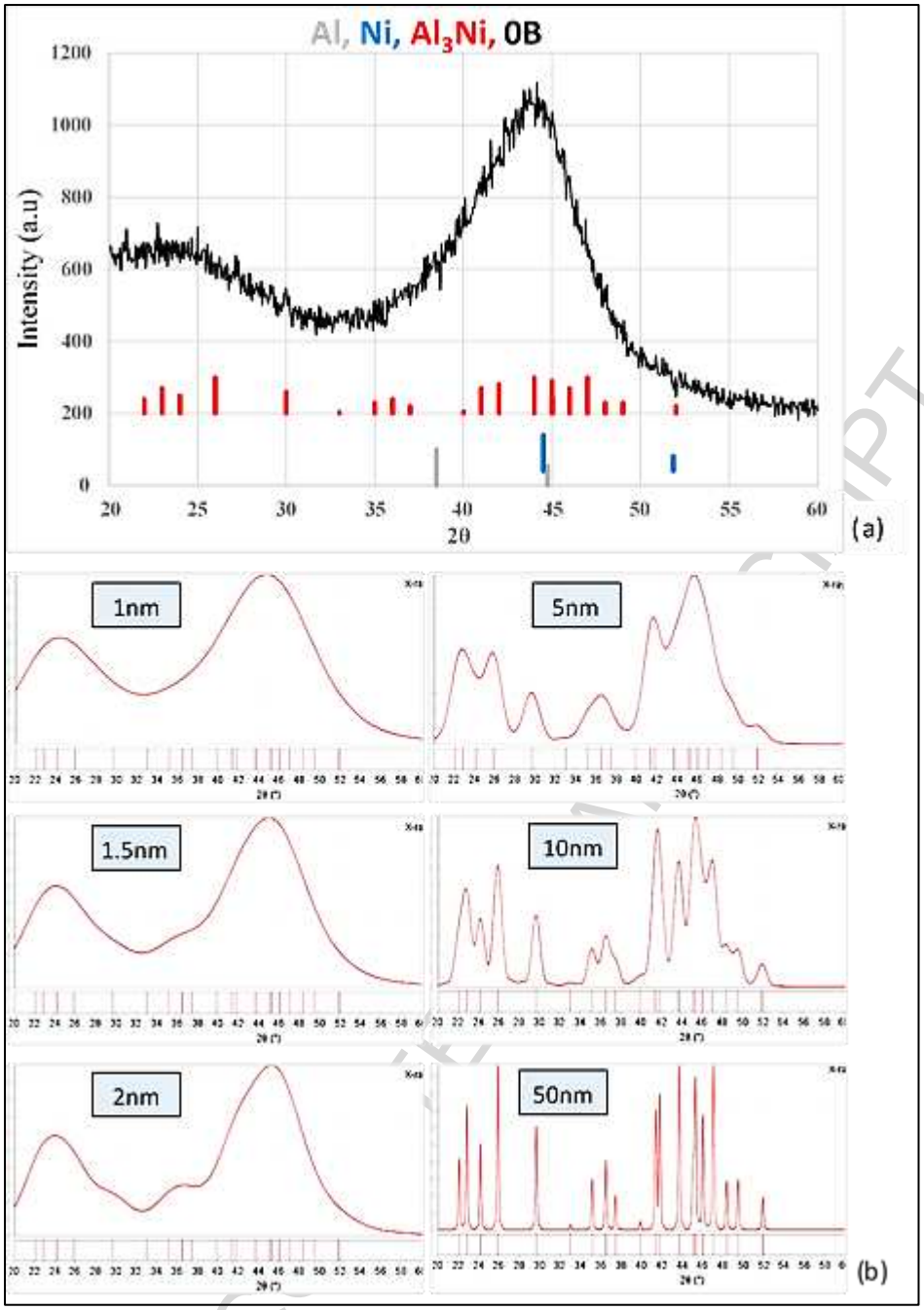

Fig. 3

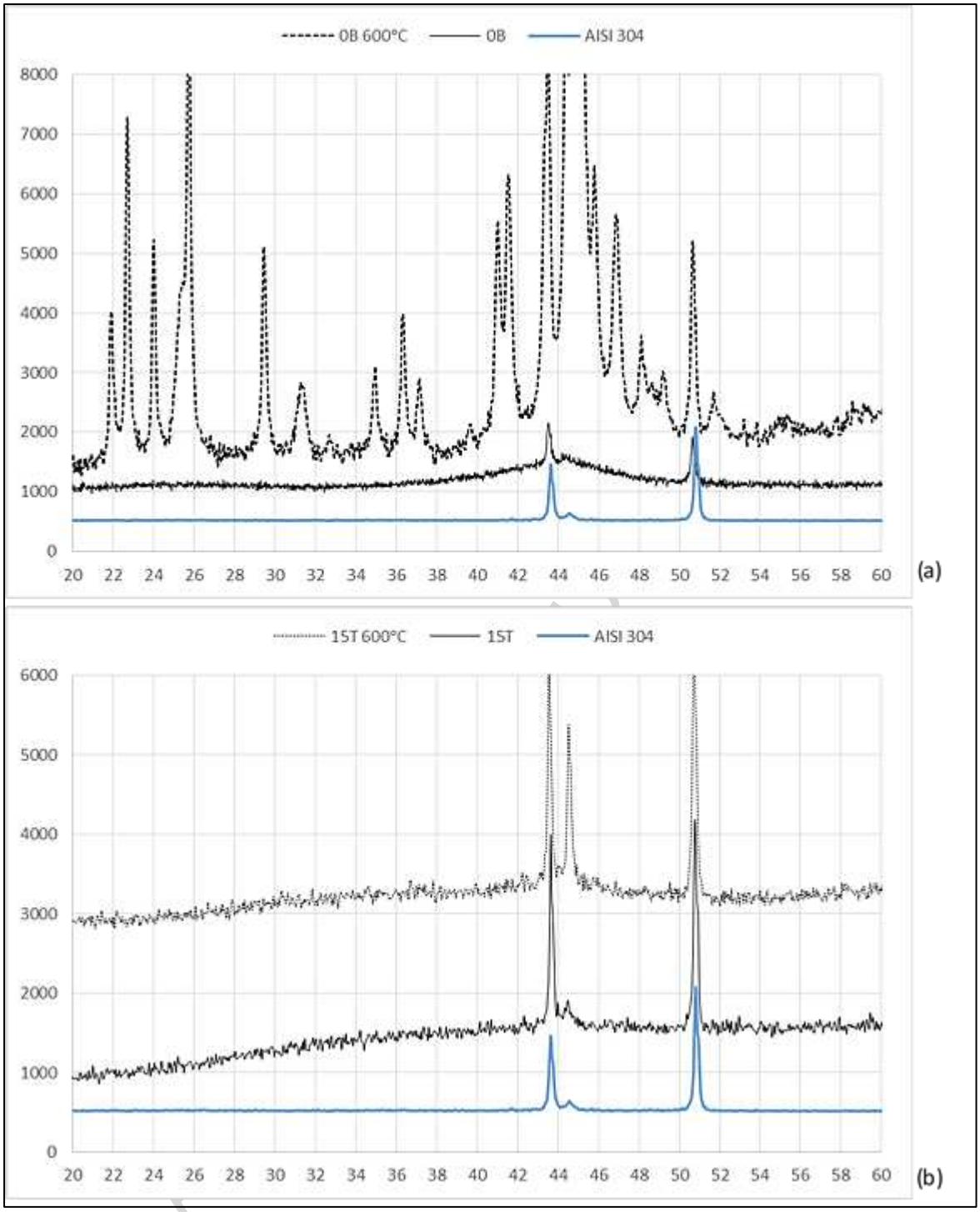

Fig. 4

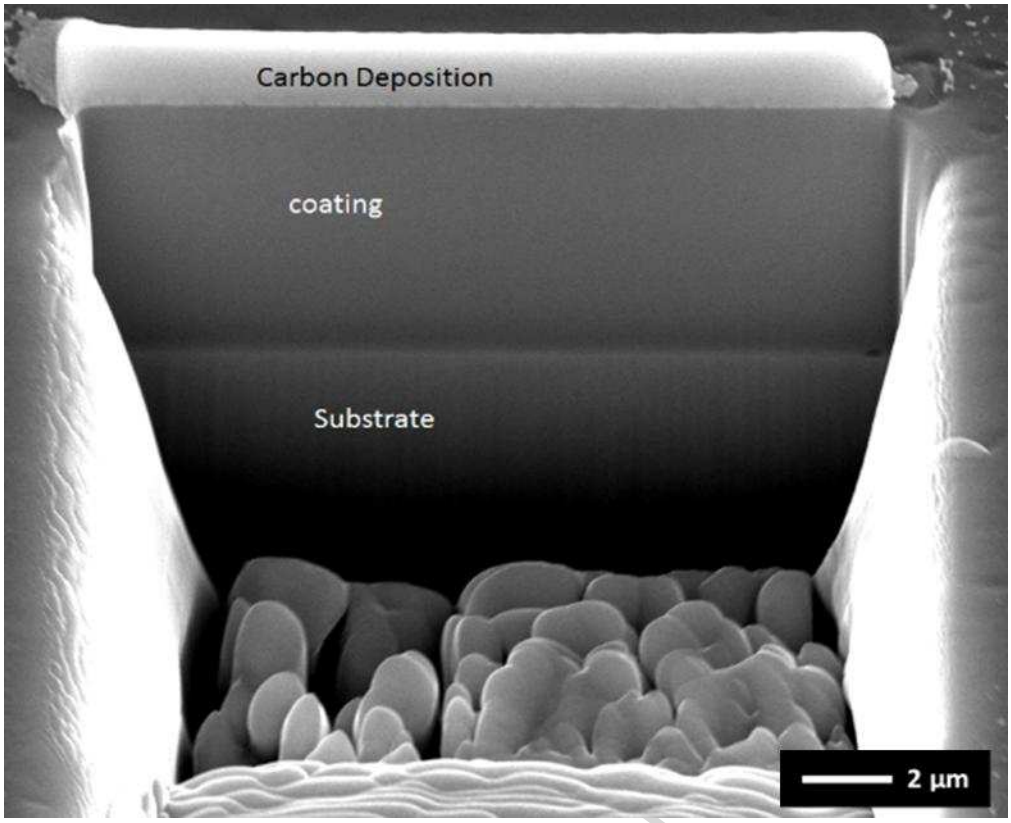

Fig. 5

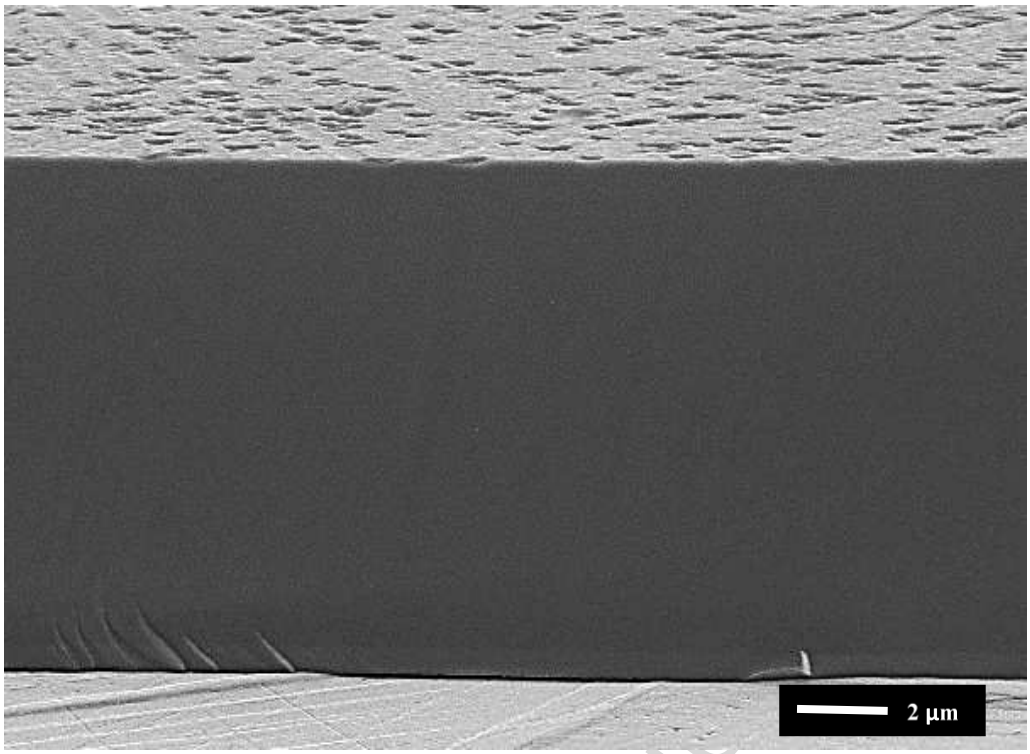

Fig. 6a

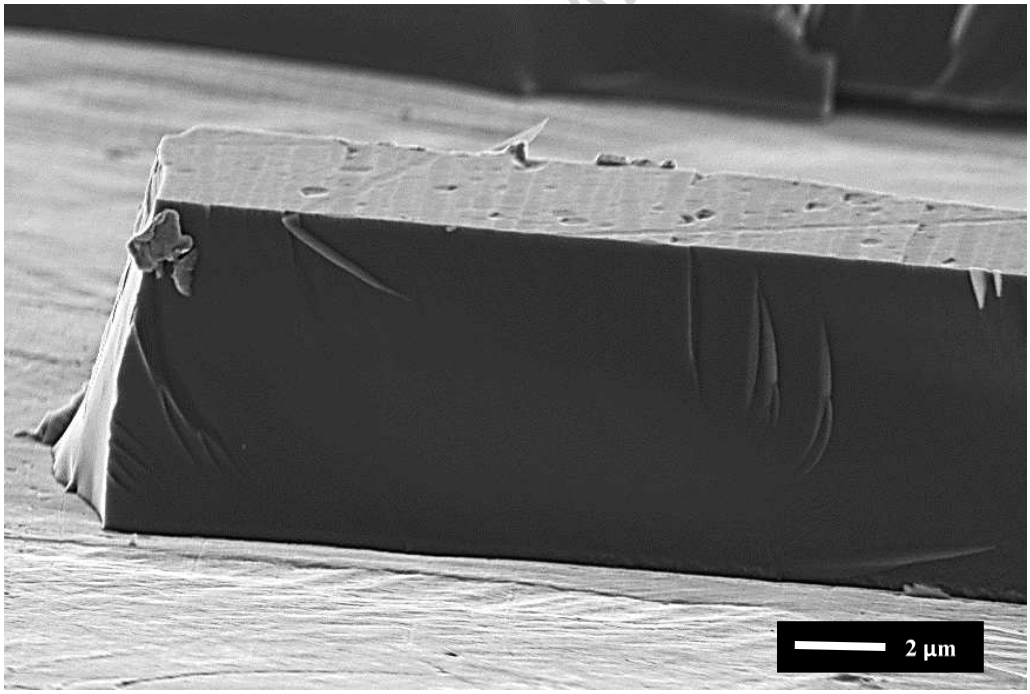

Fig. 6b

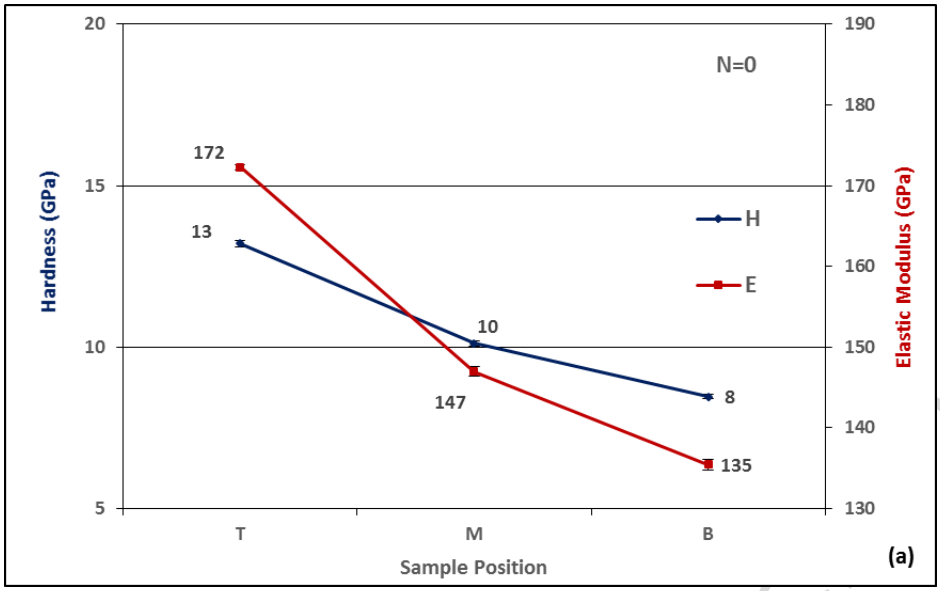

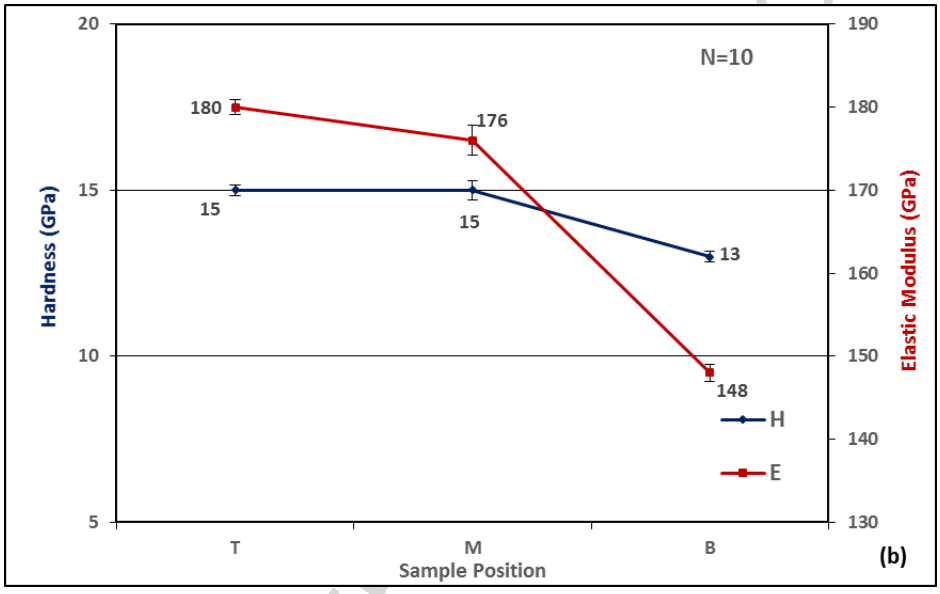

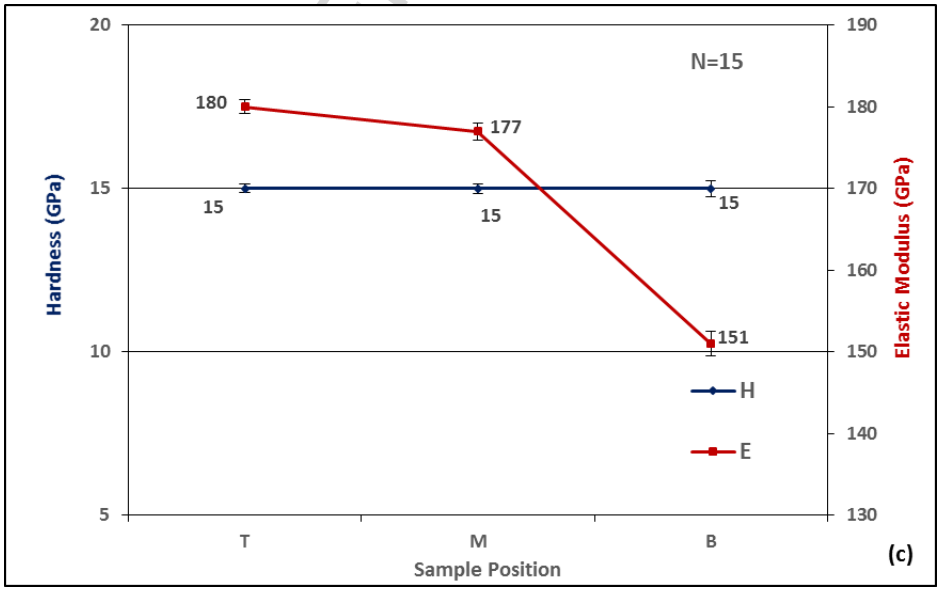

Fig. 7

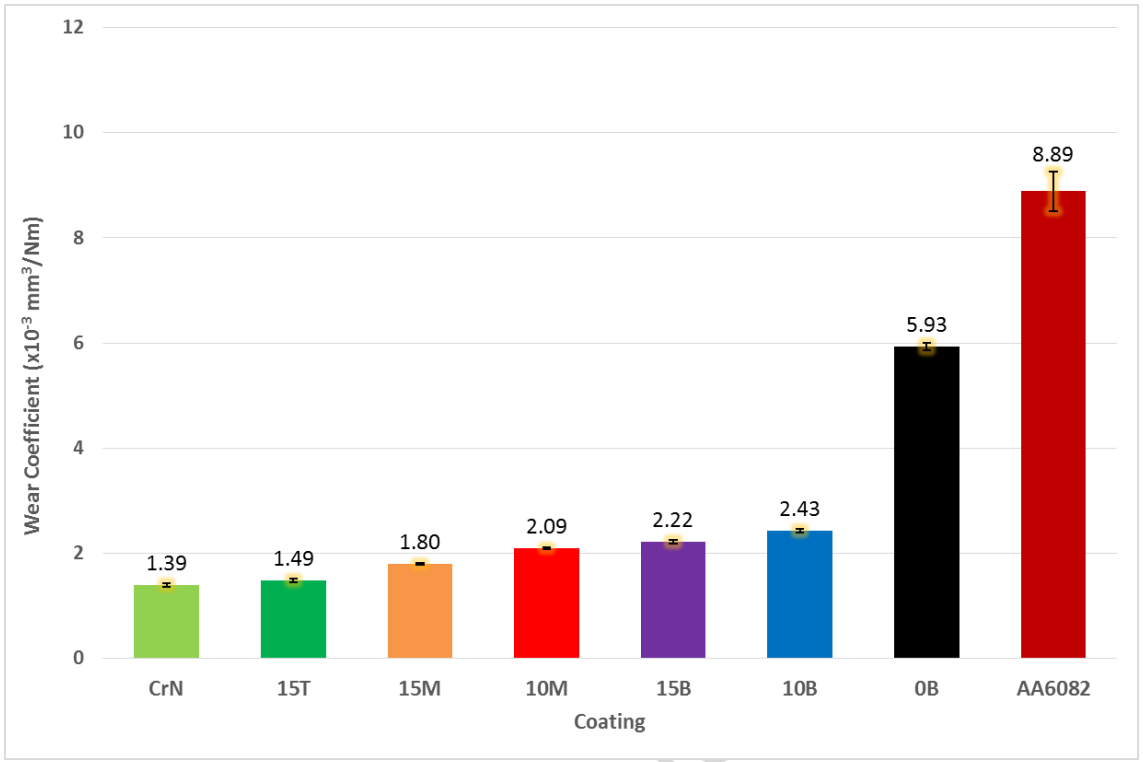

Fig. 8

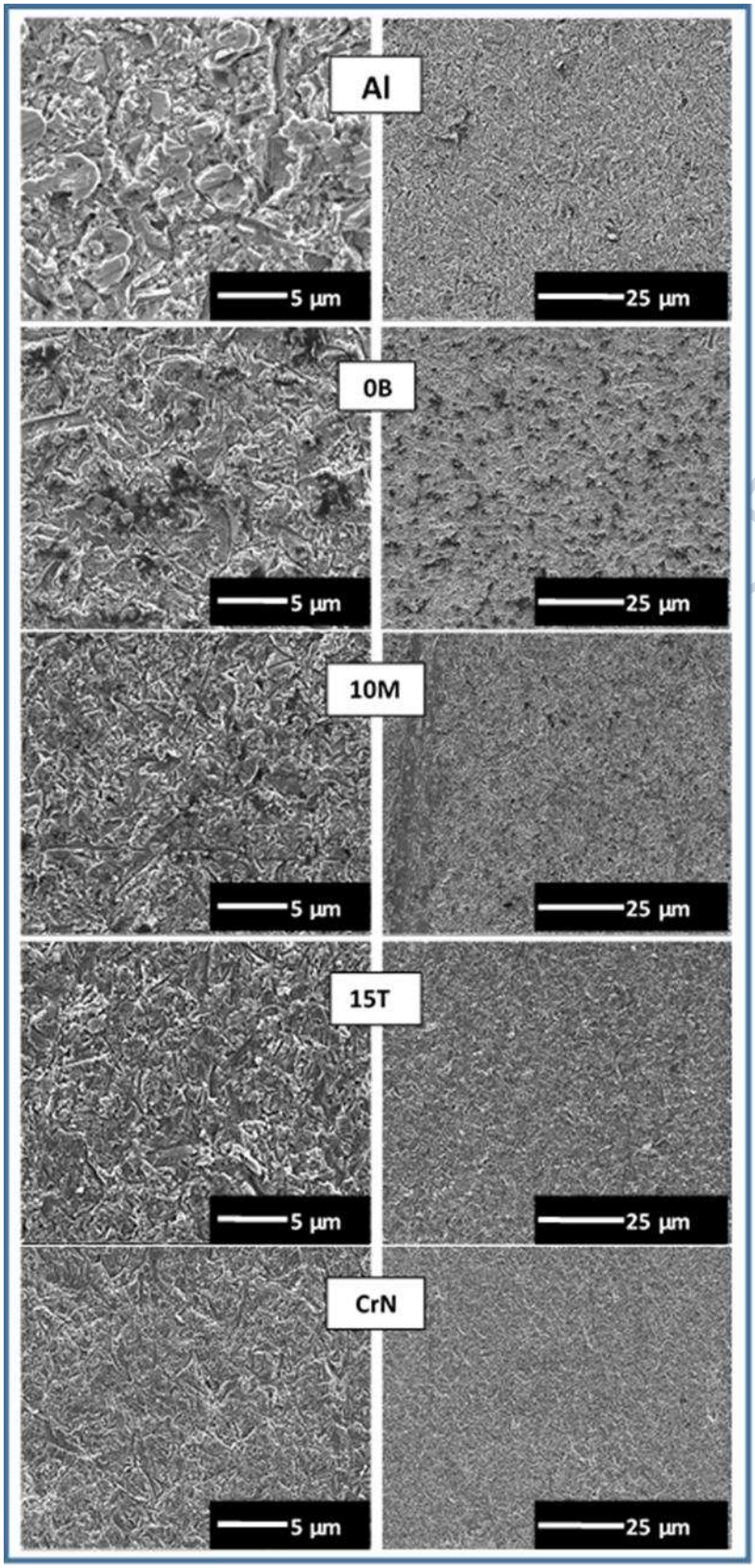

Fig. 9

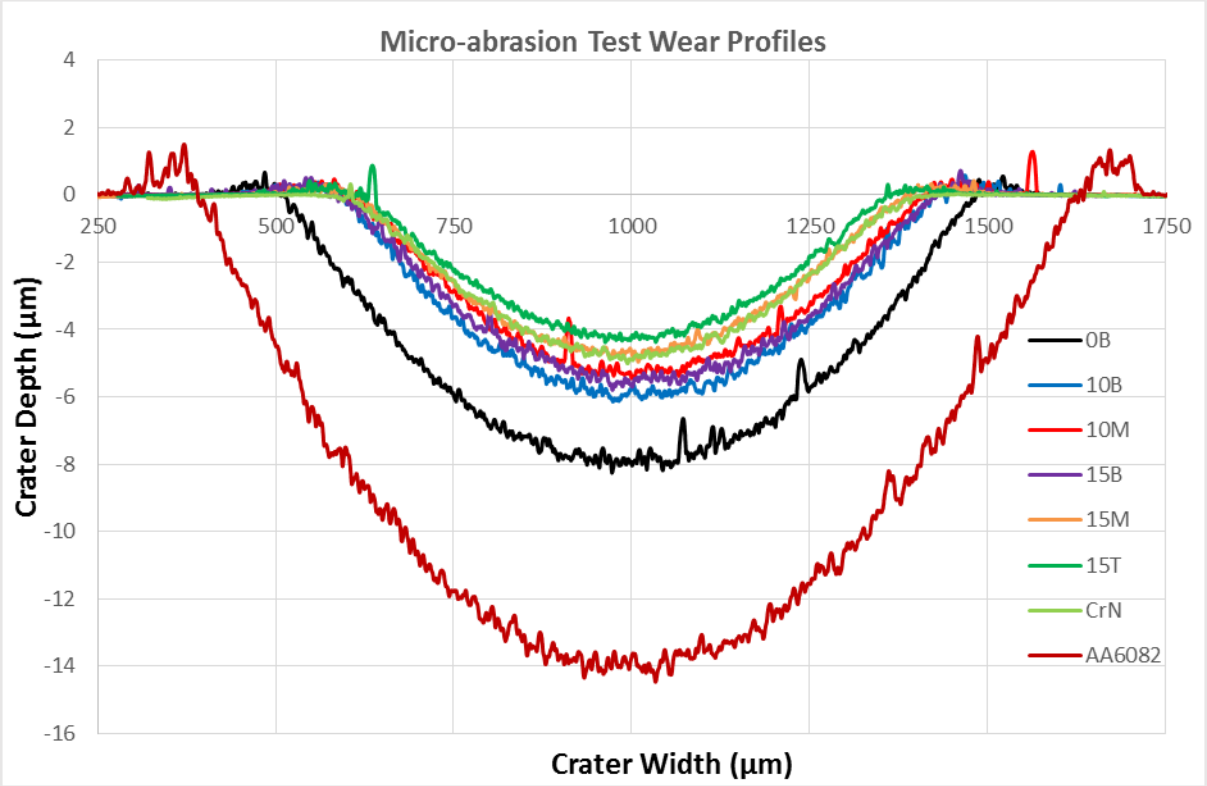

Fig. 10

I

Table 1: Sputter target composition; segment composition (and overall atomic percent)

	Al	**Ni**	**Ti**	**Si**	**B**
Al-Ni	75 (45)	25 (15)	-	-	-
Ti-Si-B	-	-	28 (11)	17 (7)	55 (22)

II

Table 2: Sample designation

0B, 10B, 10M, 15B, 15M, 15T
0, 10, and 15 refer to the chosen nitrogen flow rate (sccm) during the deposition run
B, M, and T refer to the position of the test coupon on the substrate holder facing the sputter target during deposition: bottom, middle, top, respectively (see Fig. 1)

Sample	N flow	Al	Ni	Ti	Si	B	N
TOP	0	32	11	17	10	26	0
	5	27.6	8.6	11.7	8.4	24	17.7
	10	28	8.4	9.3	6.5	19.4	27.2
	15	23.2	6.9	8.1	5.5	18	36.7
	20	23.7	7.1	6.5	4.4	14.4	42.8
MIDDLE	0	56	18.7	7.3	3.5	12.1	0.6
	5	50.7	16	6.3	2.9	10.6	12.4
	10	46.9	14.5	5.1	2.2	8.6	21.8
	15	44.8	13.4	3.8	1.2	5.8	30.3
	20	38.5	11.3	3.6	1.4	6.1	38.5
BOTTOM	0	64.8	23.1	3.8	0.3	4.9	1.7
	5	60.4	19.7	3.2	0.1	4	11.6
	10	53.6	17.4	2.5	0	3	22.9
	15	48	15.1	2.1	0	2.7	30.8
	20	42.1	12.2	1.6	0	2	41.7

III

Table 3: AlNiTiSiB(N) GDOES composition matrix (numerical values shown in atom percent) – the six coatings selected for this study are shown in the highlighted rows

IV

Table 4 A summary of results showing the potential for tuning coating properties to suit various applications/environments.

Coating	**15T**	**15M**	**10M**	**15B**	**10B**	**OB**
H (GPa)	15	15	15	15	13	8
E (GPa)	180	177	176	151	148	135
Wear coefficient ($x\ 10^{-3}$ mm^{-3}/Nm)	1.49	1.80	2.09	2.22	2.43	5.93
*OCP (V)	– 0.4	– 0.3	– 0.6	– 0.6	– 0.6	– 0.5

* Discussed in more detail in Ref. [29].